

ON THE FAST FLUCTUATIONS IN SOLAR FLARE H α BLUE WING EMISSION

M. D. DING,^{1,2} JIONG QIU,² HAIMIN WANG,² AND PHILIP R. GOODE²

Received 2000 July 15; accepted 2001 January 9

ABSTRACT

Fine temporal structures in hard X-ray and microwave emissions of solar flares have been known for many years. Recent observations with high time and spatial resolution revealed that emissions in the wings of H α could also exhibit fast (subsecond) fluctuations. We argue that such fluctuations are physically related to the small-scale injection of high-energy electrons. We explore this through numerical calculations. The energy equation and the equations for energy-level populations in hydrogen, in particular including the nonthermal collisional excitation and ionization rates, are solved simultaneously for an atmosphere impacted by a short-lived electron beam. We determine the temporal evolution of the atmospheric temperature, the atomic level populations, and the H α line intensity. We find that although the background H α wing emission is mainly formed in the photosphere, the fast fluctuations are probably produced in the chromosphere, which is penetrated by ~ 20 keV electrons. To yield H α wing fluctuations of amplitude comparable to the observations, a mean energy flux of $\sim (1-2) \times 10^{11}$ ergs cm⁻² s⁻¹ is required for the electron beam, if one adopts a Gaussian macrovelocity of 25 km s⁻¹. Such a burst contains a total energy of 10^{25} – 10^{26} ergs. These parameters are compatible with elementary flare bursts.

Subject headings: Sun: activity — Sun: atmosphere — Sun: flares

1. INTRODUCTION

It has long been recognized that solar flares may exhibit fast spectral fluctuations. After examining thousands of hard X-ray flares observed with the hard X-ray spectrometer on the *Solar Maximum Mission (SMM)*, Kiplinger et al. (1983) found hundreds of spikes of subsecond duration; the width of fastest spikes could be as short as 45 ms. Owing to the detection limit, spikes of even shorter duration may exist. Similar results were obtained by Dennis (1986). Rapid fluctuations are also frequently observed in microwave or decimetric continuum emissions (e.g., Slottje 1978; Takakura et al. 1983; Elgaroy 1986; Kliem, Karlický, & Benz 2000; Nakajima 2000). Theoretically, such fluctuations can be attributed to fine structures in the coronal magnetic field where small-scale reconnection occurs catastrophically. Aschwanden et al. (1993) proposed that a quasi-periodic injection of particles into coronal loops is the cause of decimetric and hard X-ray emissions in flares showing fast spikes. Kiplinger et al. (1984) found that the X-ray spectra of a fast spike is consistent with that predicted from a non-thermal electron beam model.

High-energy electrons are known to be responsible for the hard X-ray and microwave emissions through bremsstrahlung and gyrosynchrotron radiation, respectively. In the standard thick target model, nonthermal electrons precipitate into and deposit energy in the lower atmosphere, heating the material there, and thus producing optical line and continuum emission (e.g., Hénoux 2000). The emission closely follows the hard X-ray bursts (Canfield, Gunkler, & Ricchiazzi 1984; Canfield & Gayley 1987; Neidig et al. 1993). In particular, Gayley & Canfield (1991) investigated the relationship between flare heating and the emission in the wings of hydrogen lines. Unlike hard X-rays, optical lines need a little more time (a few tenths of a second to

seconds) to respond to the impulsive heating of a beam of electrons. Canfield & Gayley (1987) indicated that the H α blue wing varies on a timescale of ~ 0.5 s following the heating, owing to ionization imbalance.

Therefore, high time-resolution observations of flare H α emission are required for understanding the heating and energetics in the lower atmosphere of solar flares. Kämpfer & Magun (1983) studied a flare with 1.4 s resolution. Observations by Kiplinger, Dennis, & Orwig (1989) and Neidig et al. (1993) reached a time resolution of 0.5 s. Recently, Trotter et al. (2000) presented multi-wavelength observations of a flare in H α , microwave, and hard X-ray/ γ -ray wavelengths. They obtained H α images at line center with a time resolution as high as 0.2 s. By comparing the H α time profile with the hard X-ray emission, they found that the variation in H α has two components: a fast component that is proportional to the hard X-ray count rate, and a slow component that matches the time integral of the hard X-ray count rate. This provides a basic scenario of the response of the chromospheric part of the flare which is subject to heating by nonthermal electrons.

Very recently, Wang et al. (2000) used a new CCD installed at Big Bear Solar Observatory (BBSO) and successfully observed a C5.7 flare on 1999 August 23 with an unprecedented high cadence of 33 ms and a spatial resolution of 0".6. The wavelength in the observations was fixed in the H α blue wing ($\Delta\lambda = -1.3$ Å). One of the most apparent findings is that the flare footpoint, which is best correlated with the hard X-ray emission, shows high-frequency fluctuations on a timescale of a few tenths of a second. Wang et al. (2000) further proposed that these are signatures of fine temporal structures related to elementary flare bursts. Similar effort was made by Heinzel et al. (2000), who recorded high-cadence spectra of optical lines in solar flares using the Multichannel Flare Spectrograph of the Ondřejov Observatory.

The purpose of this paper is to theoretically investigate the origin of the fast fluctuations in H α by considering an atmosphere being bombarded by impulsive electron beams, which can also produce hard X-rays consistent with the

¹ Department of Astronomy, Nanjing University, Nanjing 210093, China.

² Big Bear Solar Observatory, New Jersey Institute of Technology, 40386 North Shore Lane, Big Bear City, CA 92314-9672.

observations. In the remainder of this paper, we describe the numerical method in § 2 and present the computational results in § 3. Discussions of the results and their implication in explaining the observations are given in § 4, which is followed by brief conclusions in § 5.

2. NUMERICAL METHOD

To learn how the flaring atmosphere responds to an injection of high-energy electrons requires a solution of equations of radiative hydrodynamics, i.e., to solve simultaneously the equations of mass conservation, momentum conservation, and energy conservation, together with the level population equation and radiative transfer equation (e.g., Fisher, Canfield, & McClymont 1985; Abbett & Hawley 1999). Since in the present study, our primary focus is restricted to the fast variation of the H α optical emission, the problem can be simplified. First, the hydrodynamic timescale in the chromosphere and the photosphere is tens of seconds, 2 orders of magnitude longer than the observed timescale of H α variability, which is roughly equal to the duration of electron beam pulses. Hence, we can adopt a static atmosphere, neglecting the hydrodynamic process. Second, for an electron beam-heated atmosphere, the collisional transition rates could be enhanced by several orders of magnitude in the chromosphere (Hénoux, Fang, & Gan 1993). This weakens the nonlinear coupling between the level population equation and the radiative transfer equation. In addition, the H α variability is expected to exist on a subarcsecond scale. This means that the radiation from the background atmosphere in which the flaring element is embedded becomes important in determining the mean (spatially averaged) radiative intensity, which in turn determines the radiative transition rates and the radiative cooling rate. For these two reasons, as a first-order approximation, we may solve the level population equation and the radiative transfer equation separately. When solving the former, we assume a time-independent mean radiative intensity which is computed from the background atmosphere.

The problem now reduces to a simultaneous solution of the level population equation

$$\frac{\partial n_i}{\partial t} = \sum_{j \neq i}^{N'} n_j (R_{ji} + C_{ji} + C_{ji}^B) - n_i \sum_{j \neq i}^{N'} (R_{ij} + C_{ij} + C_{ij}^B), \quad (1)$$

and the energy equation

$$\frac{\partial}{\partial t} \left[\frac{3}{2} (n_H + n_e) kT + \sum_{i=1}^{N'-1} n_i \epsilon_i + n_{N'} \chi_H \right] = H - L + L_0, \quad (2)$$

with the constraint of auxiliary equations of particle number conservation $n_H = \sum_{i=1}^{N'} n_i$ and charge conservation $n_e = n_{N'} + \zeta n_H$, where ζ refers to the contribution of other elements to the electron density and is computed in LTE. Quantity n_H is obtained from the hydrostatic equilibrium equation applied to the background atmosphere and is assumed not to change in the simulation. Quantity N' is the total number of atomic levels in the hydrogen atom ($N' = 6$ is adopted here). In equation (1), R_{ij} and R_{ji} are radiative transition rates, C_{ij} and C_{ji} are transition rates due to thermal collisions, and C_{ij}^B and C_{ji}^B are transition rates due to nonthermal collisions. In equation (2), ϵ_i is the excitation potential for bound level i , χ_H is the ionization potential, H

is the heating rate due to collision by precipitating electrons, L is the radiative cooling rate, while L_0 is an extra heating term which is equal to the radiative cooling rate in the background atmosphere. We neglect the heat conduction in equation (2) as it is less important than the electron beam heating in the chromosphere.

In the cold target approximation, the total energy deposition rate of an electron beam at column depth N is given by (Emslie 1978):

$$H = 2\pi e^4 [\xi \Lambda + (1 - \xi) \Lambda'] n_H \int_{E_N}^{\infty} \frac{F_0(E) dE}{E(1 - E_N^2/E^2)^{(2+\beta)/(4+\beta)}}, \quad (3)$$

where $F_0(E)$ is the initial flux spectrum of the injected electrons, and E_N is the minimum energy of electrons that can penetrate to depth N ; ξ is the degree of ionization, and Λ and Λ' are Coulomb logarithms for elastic and inelastic collisions, respectively. Detailed expressions of Λ and Λ' can be found in Emslie (1978).

The deposited energy is consumed in two ways. On one hand, inelastic collisions with hydrogen atoms lead to nonthermal excitation and ionization of the atoms. These have been taken into account in the level population equation. The nonthermal collisional rates are calculated according to the formulae derived by Fang, Hénoux, & Gan (1993). On the other hand, elastic collisions with ambient electrons and protons result in an increase in the kinetic temperature. (We assume that this energy is then imparted to all ambient particles which share the same temperature.) The radiative cooling consists of two parts: optically thin radiative cooling and optically thick radiative cooling, which work in high- and low-temperature regimes, respectively. The former can be expressed as

$$L_{\text{thin}} = n_e n_H P(T), \quad (4)$$

where $P(T)$ is taken from Rosner, Tucker, & Vaiana (1978). The latter is calculated as

$$L_{\text{thick}} = 4\pi \int \chi_v (S_v - J_v) dv. \quad (5)$$

The integration extends over all radiative transitions for the hydrogen atom adopted here. Cooling by the negative hydrogen ions (H^-) is also included, considering that they play a significant role in the energy balance in the lower atmosphere. Other cooling sources are neglected.

Note that the above formulae are most applicable to the case of a stationary beam. The situation is somewhat different for a pulsed beam with a short duration comparable to the electron travel time in the atmosphere. This situation was studied by Karlický & Hénoux (1992) using the particle code. However, the main contribution to the enhancement of H α wing emission is from a chromospheric layer of width, say, $\lesssim 500$ km, as will be shown in § 4.1; 20 keV electrons can transit this layer by a time of $\lesssim 6$ ms, much shorter than the duration of electron beam pulses that we will assume below. Therefore, the above formulae are still valid in the present study.

It is also necessary to check further the validity of keeping a time-independent mean radiative intensity. Through computations, we find that in the presence of an electron beam whose energy flux reaches $\sim 10^{11}$ ergs cm $^{-2}$ s $^{-1}$, the collisional rates in the chromosphere can be enhanced to be

nearly equal to or even larger than the radiative rates for most transitions except the transition between levels 1 and 2 ($\text{Ly}\alpha$), for which the difference is reduced to be within 1 order of magnitude. On the other hand, keeping J_ν time-independent leads to an overestimation of the optically thick cooling rate (see eq. [5]). However, during the peak heating, the temperature is increased so that the optically thin cooling becomes effective which is much more sensitive to the temperature variation than the optically thick cooling. Considering the above facts and assuming a small filling factor of the flaring element, we think that our approximation still yields reasonable results, although not quantitatively accurate.

In summary, we first do non-LTE calculations for a stationary background atmosphere to obtain the height distributions of n_{H} and J_ν ; when the electron beam sets in, we solve equations (1) and (2) by fixing n_{H} and J_ν to get the time-dependent variables like T , n_e , and n_i , which are then used to evaluate the line source function S_ν and optical depth τ_ν . Finally, the instantaneous $\text{H}\alpha$ line profile from the beam-heated atmosphere can be computed using the basic formula:

$$I_\nu = \int_0^\infty S_\nu e^{-\tau_\nu/\mu} d\tau_\nu/\mu = \int_0^\infty \chi_\nu S_\nu e^{-\tau_\nu/\mu} dz/\mu. \quad (6)$$

Broadening mechanisms include radiative damping, the Doppler effect, and the Stark effect. For the 1999 August 23 flare (Wang et al. 2000), $\mu \approx 0.72$ is adopted in the following computations.

3. COMPUTATIONS AND RESULTS

3.1. How Does the Electron Beam Affect the $\text{H}\alpha$ Blue Wing Emission?

In order to study the cause of rapid fluctuations in the wings of $\text{H}\alpha$, it is necessary to learn how wing emission is formed in the solar atmosphere and to what extent an electron beam can influence it. Since we are dealing with a weak flare, we adopt an atmospheric model F1 of Machado et al. (1980), as representing the background atmosphere. Figure 1 plots the height distribution of the contribution function to the emergent intensity at $\Delta\lambda = -1.3 \text{ \AA}$, i.e., the integrand of equation (6). It is clear that this emission feature is mainly formed in the photosphere. The contribution function actually contains two peaks. However, the peak in the chromosphere is nearly 3 orders of magnitude lower than that in the photosphere. However, we will show in § 4.1 that the impulsive chromospheric contribution is not trivial, and, in fact, it is more important than that of the photosphere in producing the $\text{H}\alpha$ fluctuation.

Having little knowledge of the flux spectrum of the electron beam impacting the flare atmosphere, it is convenient to assume a power-law distribution:

$$F_0(E) = \begin{cases} (\delta - 2)\mathcal{F}E_1^{\delta-2}E^{-\delta}, & E > E_1, \\ 0, & E < E_1. \end{cases} \quad (7)$$

Thus, the beam can be parameterized by an energy flux, \mathcal{F} , a low-energy cutoff, E_1 , and a spectral index, δ . Varying the energy of electrons can change their penetration depth in the atmosphere. In Figure 1, we also show the distribution of energy deposition per hydrogen atom by the electron beam for three different cases, $E_1 = 20, 50,$ and 100 keV . It is found that the electron energy is mostly deposited in the chromosphere, while a small fraction can go into the photo-

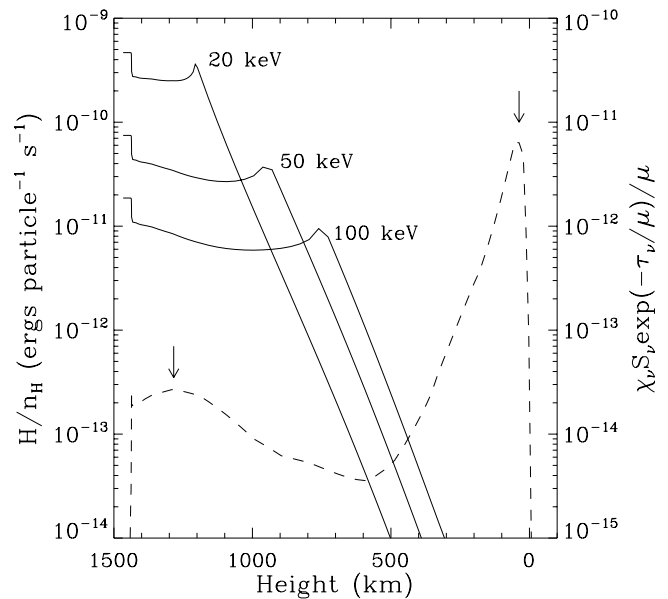


FIG. 1.—Height distribution in the atmosphere of the energy deposition rate per hydrogen atom (solid lines, left label) by electron beams of different energies ($E_1 = 20, 50,$ and 100 keV). Note that in all cases, $\mathcal{F} = 10^{11} \text{ ergs cm}^{-2} \text{ s}^{-1}$ and $\delta = 4$. Also plotted is the contribution function to the $\text{H}\alpha$ wing intensity at $\Delta\lambda = -1.3 \text{ \AA}$ (dashed line, right label), in cgs units, computed from the F1 model without nonthermal effects. The left and right arrows indicate, respectively, the chromospheric and photospheric layers that are referred to in Fig. 2.

sphere. A detailed comparison is seen in Figure 2, which displays the energy deposition rates versus E_1 in both the chromosphere ($h = 1280 \text{ km}$) and the photosphere ($h = 40 \text{ km}$). Increasing the electron energy can lessen the difference between the deposition rates in the two layers. However, the difference remains at 5 orders of magnitude in the $E_1 = 100 \text{ keV}$ case. Hence, it can be concluded that nonthermal

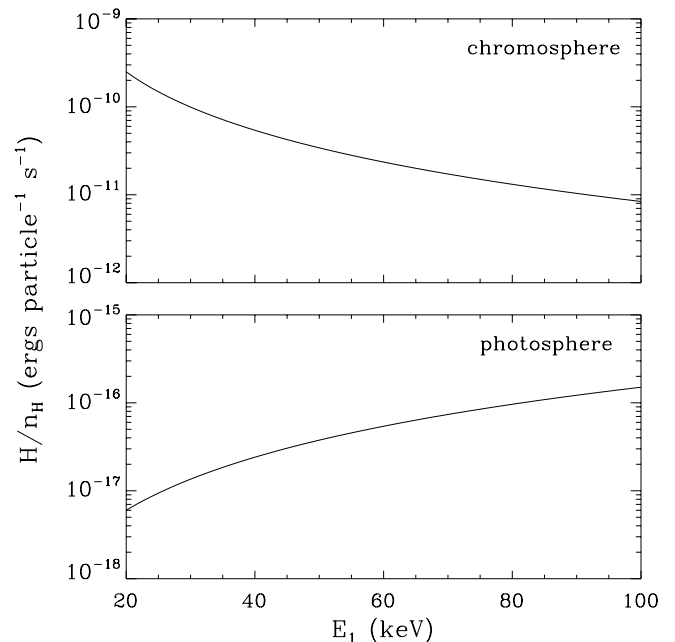


FIG. 2.—Energy deposition rate per hydrogen atom in a chromospheric layer (upper panel) and a photospheric layer (lower panel) shown in Fig. 1 as a function of the low-energy cutoff of electron beams. Note that $\mathcal{F} = 10^{11} \text{ ergs cm}^{-2} \text{ s}^{-1}$ and $\delta = 4$.

effects due to electrons are not important in the photosphere. In the following computations, we will set $E_1 = 20$ keV and $\delta = 4$ throughout, while varying the values of \mathcal{F} .

3.2. The Role of Electron Beams in Producing the H α Fluctuations

Although the observations mentioned above had a high spatial resolution of 0.6, we still cannot resolve the fine spatial structures which produced the spikes of H α wing emission. Therefore, it is unclear whether the H α fluctuations emerged from a single site or they were due to successive brightening of different sites in the spatially unresolved area. Theoretically, in the first case, repetitive magnetic reconnection should occur at the same site, leading to a periodic or quasi-periodic injection of high-energy electrons into the atmosphere. In the second case, however, magnetic reconnections are expected to take place in different small flux tubes that are mutually triggered, such as the scenario for microflares studied by Wang et al. (1999); thus, each flux tube may contain only a single pulse of the electron beam during the observing time. Of course, a real situation may also be a combination of both.

3.2.1. Case I: A Singly Pulsed Beam

In this case, a beam of electrons of short duration precipitates into the atmosphere, within a small flux tube, and produces heating there. For convenience, we may assume a triangular shape for the time variation of the energy flux, that is,

$$\mathcal{F} = \begin{cases} 4\mathcal{F}_0 \Delta t/t_d, & 0 \leq \Delta t < t_d/2, \\ 4\mathcal{F}_0(1 - \Delta t/t_d), & t_d/2 \leq \Delta t < t_d, \\ 0, & \text{otherwise,} \end{cases} \quad (8)$$

where t_d is the duration of the beam, and \mathcal{F}_0 is the mean energy flux during each pulse. Note that adopting sinusoidal or saw-tooth-shaped functions does not qualitatively alter the results below.

We have treated several cases with different values of t_d and \mathcal{F}_0 . Figure 3 shows the time variation of the kinetic temperature, the level populations of the hydrogen ground state and the ionized state at the chromospheric layer ($h = 1280$ km), and the relative enhancement of the H α line intensity at $\Delta\lambda = -1.3 \text{ \AA}$,

$$R = \Delta I_{\nu}/I_{\nu}^0 = (I_{\nu} - I_{\nu}^0)/I_{\nu}^0, \quad (9)$$

for the case of $t_d = 0.1$ s and $\mathcal{F}_0 = 10^{11}$ ergs cm $^{-2}$ s $^{-1}$. Here I_{ν} and I_{ν}^0 refer to the instantaneous and preflare intensities, respectively. The main consequences of electron beam bombardment can be briefly described as follows. When the electron beam initially precipitates downward, the atmospheric temperature rises, and the hydrogen atoms are excited and ionized through thermal and nonthermal collisions; thus, the ground level is depopulated, while the excited and ionized levels become overpopulated with respect to the preflare status. Accordingly, the H α source function is enhanced, which leads finally to an excess emission in the H α line wing. If there is no extra energy input after the beam, the atmosphere will relax to its original status in a time, which is determined by the radiative cooling rate. The cooling is quite efficient when $T \gtrsim 10^4$ K, but becomes slow when $T \lesssim 10^4$ K, during which only the optically thick cooling matters.

An important parameter is the amplitude of relative enhancement of the H α wing intensity, denoted as R_0 .

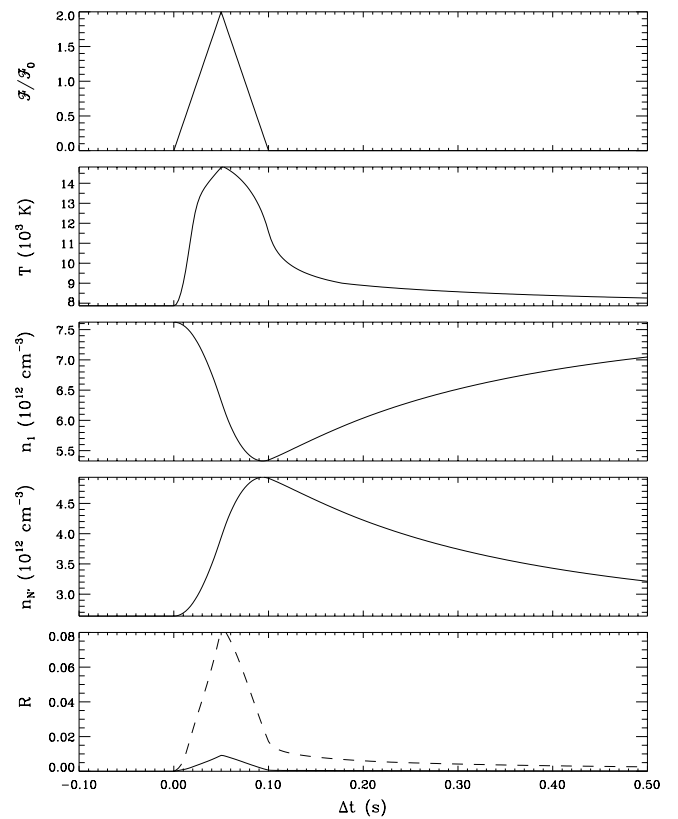


FIG. 3.—Time evolution of physical parameters in a chromospheric layer (indicated in Fig. 1) in response to an impulsive heating by an electron beam ($\mathcal{F}_0 = 10^{11}$ ergs cm $^{-2}$ s $^{-1}$, $E_1 = 20$ keV, and $\delta = 4$). $\Delta t = 0$ refers to the beam onset time. From top to bottom, the parameters shown are the energy flux of the beam, atmospheric temperature, hydrogen ground state population, population of ionized hydrogen, and relative enhancement of the H α line intensity at $\Delta\lambda = -1.3 \text{ \AA}$. In the bottom panel, the dashed curve is obtained after convolving the line profiles (both I_{ν} and I_{ν}^0) with a Gaussian macrovelocity of 25 km s $^{-1}$, while the solid curve refers to the case without invoking any macrovelocity.

Figure 4 shows the effects on R_0 of varying either t_d or \mathcal{F}_0 . A fact which deserves mention is that the value of R_0 depends slightly on the beam duration. A beam of shorter duration tends to produce less H α variations than a beam of longer duration if the mean energy flux is unchanged. This can be easily understood since the total energy input is smaller in the former case, and more importantly, the response of the atmosphere depends on the impulsiveness of the electron beam. On the other hand, if the time duration is fixed, varying the energy flux has a direct consequence on the extent of the heating and, thus, the enhancement of H α emission.

The atmosphere during flares may be in a turbulent state induced by the impulsive heating. Usually, in the modeling of flare atmospheres, a macroturbulent velocity is invoked to smooth the theoretical profile for a better comparison with observations (e.g., Gan & Fang 1987; Ding & Fang 1993). The nature of such macroturbulence is not very clear and may be attributed to the superposition of some flare-associated macroscopic velocity fields. In the present study, the extent of macroturbulence is crucial to the H α profile since it can redistribute the emission at line core to the line wings. Therefore, we have assumed a Gaussian macrovelocity of 25 km s $^{-1}$ to convolve with the computed profiles. Figure 5 shows an example of the effect of Gaussian

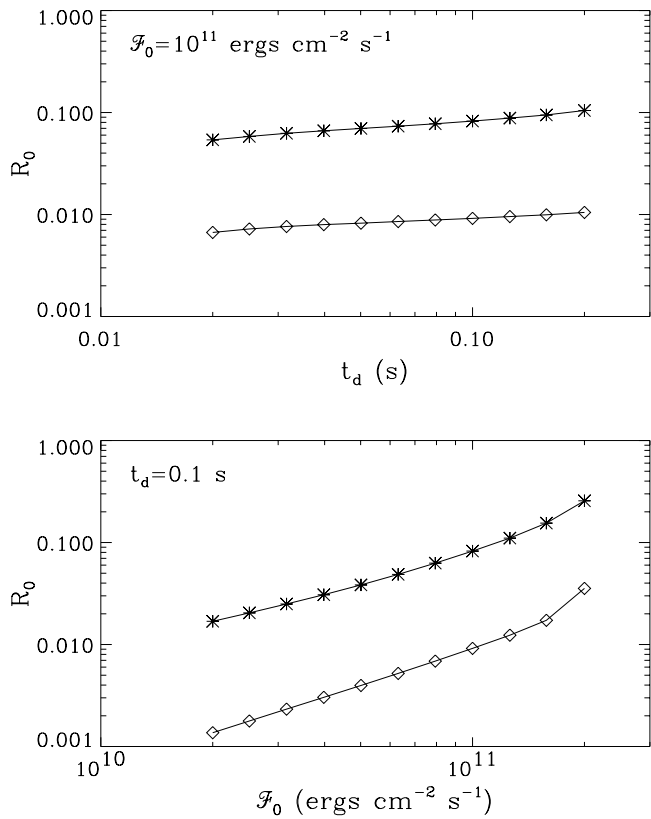


FIG. 4.—Effects of varying the duration (t_d , upper panel) and mean energy flux (\mathcal{F}_0 , lower panel) of electron beams on the amplitude of relative enhancement of the $H\alpha$ wing intensity. In each panel, the upper curve is obtained by assuming a Gaussian macrovelocity of 25 km s^{-1} , while the lower curve refers to the case without any macrovelocity.

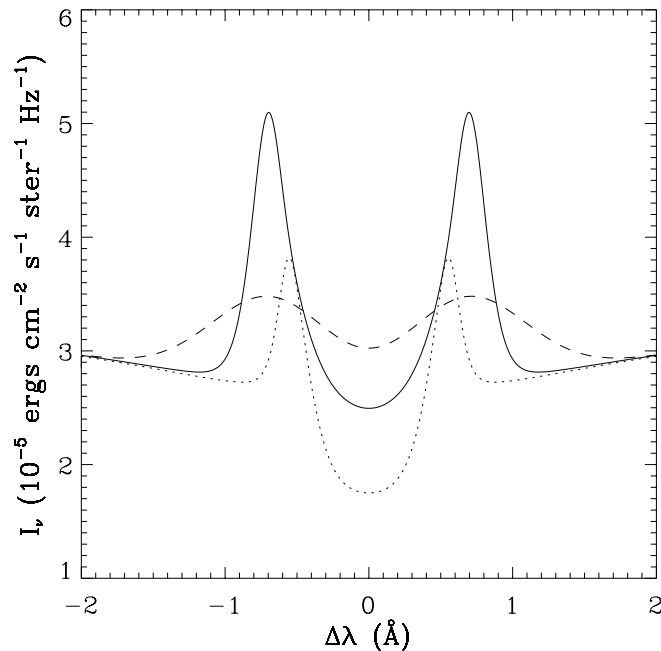


FIG. 5.— $H\alpha$ line profile from the atmosphere at the peak time of the electron beam ($\Delta t = 0.05 \text{ s}$, solid line) and that before the beam onset ($\Delta t = 0$, dotted line) for the case shown in Fig. 3. Also plotted is the profile at the peak time convolved with a Gaussian macrovelocity of 25 km s^{-1} (dashed line), showing a significant increase of the line wing intensity.

macrobroadering on the line profile. The line wing enhancement obtained in this way is also plotted in Figures 3 and 4 together with that in the case of no macrovelocity. Strikingly, yet conceivably, the former is nearly 1 order of magnitude greater than the latter.

In the above computations, the parameter R_0 is defined at $\Delta\lambda = -1.3 \text{ \AA}$ (the blue wing). This is only because the observations were made at this wavelength. Note that the same results can be obtained at $\Delta\lambda = 1.3 \text{ \AA}$ (the red wing) as we have assumed a static atmosphere. When considering a bandpass of 0.25 \AA , as in the observations (Wang et al. 2000), we find that the value of R_0 changes very slightly by $\lesssim 3\%$.

3.2.2. Case II: A Periodically Pulsed Beam

For repetitive injections of electrons at a same place, we may mimic the time variation of the energy flux as a periodic function by introducing a new parameter, the repetition time of the pulses. Observations of the 1999 August 23 flare have revealed that the most probable repetition time is $0.3\text{--}1.0 \text{ s}$, while the power spectrum shows that even shorter ($< 0.3 \text{ s}$) repetition times may exist (Wang et al. 2000). Figure 6 shows an example of the atmosphere heated by a multipulsed beam.

The basic difference between the case of multiple pulses and the case of a single pulse is that the former involves a long-term evolution of the atmosphere, in addition to the impulsive features. As long as the mean input energy, averaged over one time period, is larger than the radiative cooling rate, the mean atmospheric temperature will continue to rise until they get balanced. This is most evident in

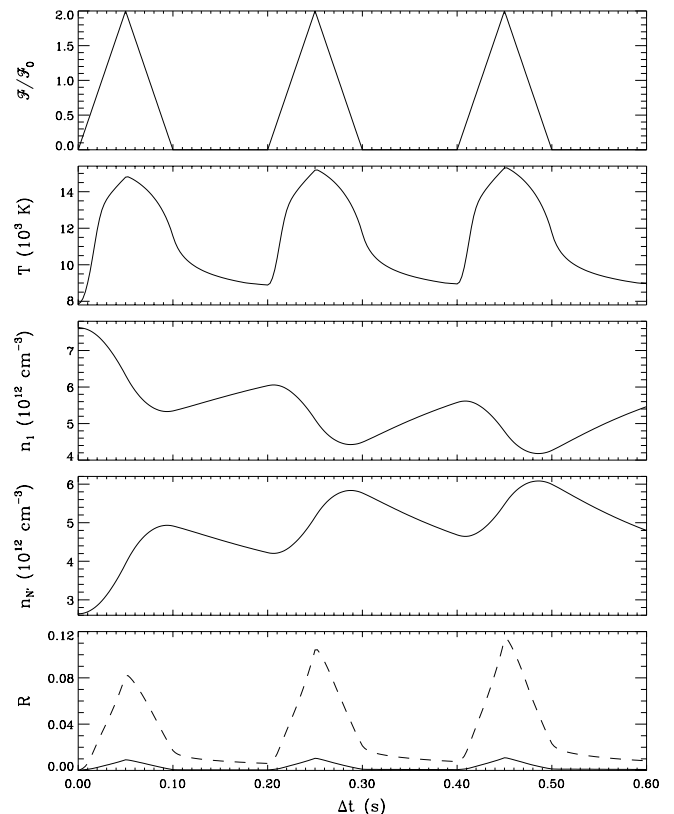


FIG. 6.—Same as Fig. 3, but for the case of a periodically pulsed electron beam ($\mathcal{F}_0 = 10^{11} \text{ ergs cm}^{-2} \text{ s}^{-1}$, $E_1 = 20 \text{ keV}$, and $\delta = 4$). The repetition time of beam pulses is 0.2 s .

cases of high-repetition rates and large beam fluxes. Such gradual heating results in a slightly modified background atmosphere, which leads to a slowly varying component of H α emission, as indicated by Trottet et al. (2000); the amplitude of H α fluctuations could vary somewhat with the background atmosphere, as shown in Figure 6.

The chromospheric response to consecutive short-duration beam pulses has also been studied by Heinzel (1991) and Heinzel & Karlický (1992). In the computations of Heinzel (1991), the author treated the radiative rates using the escape probability technique. He did not solve the energy equation while adopting a prescribed time profile of temperature. The H α line intensity was calculated from a constant-property flaring layer. We find that our results concerning the temporal variation of the H α emission are in qualitative agreement with the results of Heinzel (1991). A quantitative comparison is impractical owing to the differences in the computational methods, as described above, and in some key input parameters like the pulse duration, etc.

4. DISCUSSION

4.1. Where Are the H α Fluctuations Formed?

As mentioned above, an electron beam not only contributes to the heating of the atmosphere but also causes a direct collisional excitation and ionization of the ambient hydrogen atoms (Hudson 1972; Lin & Hudson 1976). This effect has been shown to be important in both theoretical flare models (Ricchiazzi & Canfield 1983) and semiempirical models (Abouadarham & Héroux 1986, 1987; Fang et al. 1993, 1995), as well as in powering the continuum emission of white-light flares (Ding, Fang, & Yun 1999) and producing the Ellerman bombs (Ding, Héroux, & Fang 1998). During an electron beam impact, the degree of ionization in the chromosphere can be greatly enhanced as compared to a purely thermal case. The impulsive variation of the H α wing intensity following the energy flux of the electron beam is due to the nonthermal effect and the effect of the temperature variation, which both change the line source function where the H α line wing is formed.

We have shown that ~ 20 keV electrons do not penetrate to the photosphere and produce direct heating there. The photosphere could be indirectly heated through backwarming by enhanced chromospheric radiations (Machado, Emslie, & Avrett 1989; Metcalf, Canfield, & Saba 1990). Although this effect is not included in the present model, it does not affect our results since the radiatively heated layers have no impulsive nature.

To quantitatively assess which layer contributes most to the relative enhancement of the H α wing emission, we derive a transfer equation for the parameter R ,

$$\mu \frac{dR}{dz} = -\chi_R(R - S_R), \quad (10)$$

following the method of Magain (1986) in discussing the formation of line depression. In equation (10), χ_R and S_R are the “effective absorption coefficient” and the “effective source function,” respectively. They are defined as

$$\chi_R = \Delta\chi_v + j_v^0/I_v^0, \quad (11)$$

$$S_R = (\Delta j_v - \Delta\chi_v I_v^0)/(j_v^0 + \Delta\chi_v I_v^0), \quad (12)$$

where a superscript 0 refers to the value at preflare status, $\Delta j_v = j_v - j_v^0$, and $\Delta\chi_v = \chi_v - \chi_v^0$. Therefore, the relative enhancement of the H α intensity can also be computed as

$$R = \int_0^\infty S_R e^{-\tau_R/\mu} d\tau_R/\mu = \int_0^\infty \chi_R S_R e^{-\tau_R/\mu} dz/\mu, \quad (13)$$

where $d\tau_R = \chi_R dz$. The integrand in equation (13) refers to the contribution function (per unit depth) to the parameter R . This function is plotted in Figure 7 for the case shown in Figure 3, but at $\Delta t = 0.05$ s (the peak time of energy flux). Not surprisingly, the contribution function to R peaks in the chromosphere, not in the photosphere, contrary to the contribution function to I_v . This consolidates our conclusion that the H α wing fluctuations originate from the chromosphere, though the photosphere contributes more to the background intensity.

4.2. The Nature of Elementary Bursts

A solar flare may be composed of many small-scale bursts called elementary bursts. The avalanche model of flares by Lu & Hamilton (1991) accounts for the power law for the flare frequency distribution. Through a comparison with observations, Lu et al. (1993) were able to obtain a reasonable fit with an elementary event energy of $\sim 3 \times 10^{25}$ ergs and duration of ~ 0.3 s. LaRosa & Moore (1993) proposed an MHD turbulent cascade model for energizing the electrons. This model suggests that outflows from driven magnetic reconnection can be unstable and turbulent so that the kinetic energy is rapidly dissipated through turbulent cascade. The largest eddy, whose diameter is 10^2 – 10^3 km, can produce $\sim 10^{26}$ ergs of energized electrons in ~ 0.3 s. LaRosa, Moore, & Shore (1994) further pointed out that Fermi acceleration can account for the electron acceleration, from 0.1 keV to approximately 25 keV on the

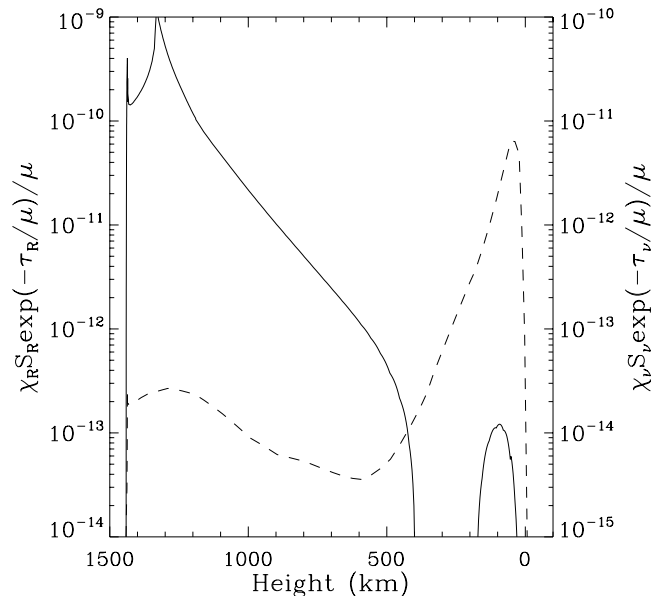


FIG. 7.—Contribution function to the relative enhancement of H α wing intensity (solid line, left label) in a perturbed atmosphere shown in Fig. 3 (at $\Delta t = 0.05$ s), in contrast to the contribution function to the absolute H α wing intensity (dashed line, right label) in the background atmosphere. The data are in cgs units.

subsecond timescales. A detailed analysis of the elementary structures in solar flares was recently done by Aschwanden, Dennis, & Benz (1998).

If the model of LaRosa & Moore (1993) is correct, the energy flux of injected electrons is as high as 10^{10} – 10^{12} ergs $\text{cm}^{-2} \text{s}^{-1}$, even in the case that electrons are isotropically directed. This means that in a solar flare, the electron beams may be highly concentrated rather than distributed in a broad region.

4.3. Comparison with Observations

Analysis of H α wing emission for the 1999 August 23 flare has clearly revealed the existence of fast fluctuations in one flare kernel (Wang et al. 2000). For reference, we plot in Figure 8 the contrast of H α wing emission, with the slowly varying component removed, in kernels K1 and K2 of this flare. Kernel K1 shows 10 fluctuation peaks whose amplitude is larger than 3 times the noise level. They yield a mean amplitude of $\sim 3\%$. In contrast, kernel K2 shows fluctuations of a much lower amplitude, which are probably owing to pure noise.

The contrast of H α wing emission plotted in Figure 8 is actually a mean value over the flare ribbon. Assuming, further, that the filling factor of small-scale bursts is ~ 0.1 – 0.5 , the emission contrast within each burst can be as high as $\sim 6\%$ – 30% . Judging from Figure 4, in the case without any macrovelocity, it is really hard to obtain H α fast fluctuations of such a large amplitude even for very strong electron beams. However, if there exists a macrovelocity, it is possible to produce fluctuations comparable to those in the observations. In this case, we require a mean energy flux of $\sim (1\text{--}2) \times 10^{11}$ ergs $\text{cm}^{-2} \text{s}^{-1}$ if we adopt a Gaussian macrovelocity of 25 km s^{-1} , as above. If the beam has a spatial size of $\lesssim 1''$, then the total energy carried by electrons during each burst amounts to $\sim 10^{25}$ – 10^{26} ergs.

For each burst, we can expect a hard X-ray flux whose time profile is almost identical to the electron injection function (Aschwanden, Schwartz, & Dennis 1998) and is, thus, similar to the enhancement of the H α wing intensity, as is shown in Figure 3. Since the BATSE hard X-ray observations for the 1999 August 23 flare lacks sufficient tempo-

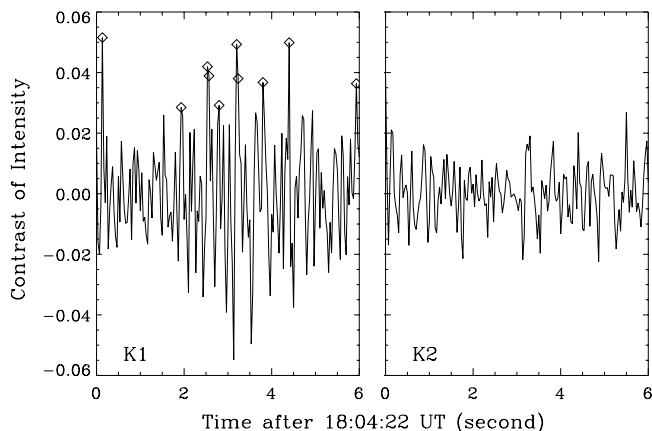


FIG. 8.—Mean contrast of H α wing emission, with the slowly varying component filtered out, in two kernels of the 1999 August 23 flare. In kernel K1 (*left panel*), spikes with an amplitude larger than 3σ level are marked by diamonds. In contrast, kernel K2 (*right panel*) shows only pure noises.

ral resolution (the high-cadence mode was not triggered), a direct comparison between the fine structures in both H α and hard X-ray is not possible. However, the similarity between the smoothed time profiles in these two wavelengths (Wang et al. 2000) is compatible with the scenario that the flare could be a superposition of many small-scale bursts.

5. CONCLUSIONS

We have performed numerical calculations of the response of an atmosphere bombarded by an impulsive electron beam of short (subsecond) duration. This work aims to explain the fast variations of the H α wing emission observed in a solar flare on 1999 August 23 (Wang et al. 2000) as being due to the injection of such short-lived electron beams. We solve simultaneously, at each depth, the energy equation and the equations for level population in hydrogen, particularly taking into account the collisional excitation and ionization by the nonthermal electrons. The calculations are based on a static atmosphere since the chromospheric hydrodynamic timescale is much longer than the injection time. The code predicts the time evolution of the atmospheric temperature, the atomic level populations, and finally the H α line intensity. Our main conclusions are summarized as follows:

1. Although in the background atmosphere, the H α wing emission at $\Delta\lambda = -1.3 \text{ \AA}$ is formed mainly in the photosphere, the H α fluctuations revealed in the observations are indeed produced by the perturbation in the chromosphere. This implies that $\sim 20 \text{ keV}$ electrons, which can only penetrate to the chromosphere, could be a viable agent in producing the H α fluctuations. There is no need to invoke very energetic ($\sim 100 \text{ keV}$ or even higher) electrons that can penetrate deeper but would be unlikely in this small flare.

2. The effects of nonthermal collisional excitation and ionization play an important role in producing the excess H α wing emission, in complement to the effect of temperature rise. Bombardment by an electron beam greatly enhances the chromospheric electron density and makes the Stark broadening more obvious. Nonthermal origin is more likely than thermal origin because the former has a more impulsive nature.

3. Observations cannot distinguish two possibilities: a small flux tube with repetitive injection of electrons or superposition of many small flux tubes triggered successively. For each pulse of electron injection, there is no essential difference between these two cases, only that in the former, the background atmosphere could be heated gradually until the radiative cooling can balance the mean energy input rate.

4. Observations show a mean amplitude of H α emission contrast of $\sim 3\%$. Assuming a filling factor of ~ 0.1 – 0.5 , this requires electron beams with a mean energy flux of $\sim (1\text{--}2) \times 10^{11}$ ergs $\text{cm}^{-2} \text{s}^{-1}$, if one adopts a Gaussian macrovelocity of 25 km s^{-1} . The total energy carried by nonthermal electrons during each burst is estimated to be $\sim 10^{25}$ – 10^{26} ergs. Hence, such beams belong to typical elementary bursts.

We note that in order to more closely relate the variability of the H α emission to the electron injection, high-cadence observations in both H α and hard X-ray are

required. Cross-correlation analysis of fast features made in these two wavebands is of great interest for the future.

We would like to thank the referee for a careful reading and insightful comments on the paper. This work was sup-

ported by NSF under grant INT 96-03534 and ATM 97-14796 and by NASA under NAG5-9682. M. D. D. was also supported by NSFC under grant 10025315 and by TRAPOYT. He thanks the staff of BBSO for kind help during his visit there.

REFERENCES

- Abbett, W. P., & Hawley, S. L. 1999, *ApJ*, 521, 906
 Abudarham, J., & Hénoux, J.-C. 1986, *A&A*, 168, 301
 ———. 1987, *A&A*, 174, 270
 Aschwanden, M. J., Benz, A. O., Dennis, B. R., & Gaizauskas, V. 1993, *ApJ*, 416, 857
 Aschwanden, M. J., Dennis, B. R., & Benz, A. O. 1998, *ApJ*, 497, 972
 Aschwanden, M. J., Schwartz, R. A., & Dennis, B. R. 1998, *ApJ*, 502, 468
 Canfield, R. C., & Gayley, K. G. 1987, *ApJ*, 322, 999
 Canfield, R. C., Gunkler, T. A., & Ricchiazzi, P. J. 1984, *ApJ*, 282, 296
 Dennis, B. R. 1986, in *Solar Flares and Coronal Physics Using P/OF as a Research Tool*, ed. E. Tandberg-Hanssen, R. M. Wilson, & H. S. Hudson (NASA CP-2421; Washington, DC: NASA), 67
 Ding, M. D., & Fang, C. 1993, *Sol. Phys.*, 147, 305
 Ding, M. D., Fang, C., & Yun, H. S. 1999, *ApJ*, 512, 454
 Ding, M. D., Hénoux, J.-C., & Fang, C. 1998, *A&A*, 332, 761
 Elgaroy, O. 1986, *Sol. Phys.*, 104, 43
 Emslie, A. G. 1978, *ApJ*, 224, 241
 Fang, C., Hénoux, J.-C., & Gan, W. Q. 1993, *A&A*, 274, 917
 Fang, C., Hénoux, J.-C., Hu, J., Xue, Y.-Z., Gao, X.-F., & Fu, Q.-J. 1995, *Sol. Phys.*, 157, 271
 Fisher, G. H., Canfield, R. C., & McClymont, A. N. 1985, *ApJ*, 289, 414
 Gan, W. Q., & Fang, C. 1987, *Sol. Phys.*, 107, 311
 Gayley, K. G., & Canfield, R. C. 1991, *ApJ*, 380, 660
 Heinzel, P. 1991, *Sol. Phys.*, 135, 65
 Heinzel, P., & Karlický, M. 1992, in *Coronal Streamers, Coronal Loops, and Coronal and Solar Wind Composition*, ed. C. Mattok (ESA SP-348; Noordwijk: ESA), 237
 Heinzel, P., Karlický, M., Kotrč, P., & Kupryakov, Yu. A. 2000, in *ASP Conf. Ser. 206, High Energy Solar Physics: Anticipating HESSI*, ed. R. Ramaty & N. Mandzhavidze (San Francisco: ASP), 289
 Hénoux, J.-C. 2000, in *ASP Conf. Ser. 206, High Energy Solar Physics: Anticipating HESSI*, ed. R. Ramaty & N. Mandzhavidze (San Francisco: ASP), 27
 Hénoux, J.-C., Fang, C., & Gan, W. Q. 1993, *A&A*, 274, 923
 Hudson, H. S. 1972, *Sol. Phys.*, 24, 414
 Kämpfer, N., & Magun, A. 1983, *ApJ*, 274, 910
 Karlický, M., & Hénoux, J.-C. 1992, *A&A*, 264, 679
 Kiplinger, A. L., Dennis, B. R., Frost, K. J., & Orwig, L. E. 1984, *ApJ*, 287, L105
 Kiplinger, A. L., Dennis, B. R., Frost, K. J., Orwig, L. E., & Emslie, A. G. 1983, *ApJ*, 265, L99
 Kiplinger, A. L., Dennis, B. R., & Orwig, L. E. 1989, in *Max '91 Workshop 2: Developments in Observations and Theory for Solar Cycle 22*, ed. R. M. Winglee & B. R. Dennis (Greenbelt: NASA), 346
 Kliem, B., Karlický, M., & Benz, A. O. 2000, *A&A*, 360, 715
 LaRosa, T. N., & Moore, R. L. 1993, *ApJ*, 418, 912
 LaRosa, T. N., Moore, R. L., & Shore, S. N. 1994, *ApJ*, 425, 856
 Lin, R. P., & Hudson, H. S. 1976, *Sol. Phys.*, 50, 153
 Lu, E. T., & Hamilton, R. J. 1991, *ApJ*, 380, L89
 Lu, E. T., Hamilton, R. J., McTiernan, J. M., & Bromund, K. R. 1993, *ApJ*, 412, 841
 Machado, M. E., Avrett, E. H., Vernazza, J. E., & Noyes, R. W. 1980, *ApJ*, 242, 336
 Machado, M. E., Emslie, A. G., & Avrett, E. H. 1989, *Sol. Phys.*, 124, 303
 Magain, P. 1986, *A&A*, 163, 135
 Metcalf, T. R., Canfield, R. C., & Saba, J. L. R. 1990, *ApJ*, 365, 391
 Nakajima, H. 2000, in *ASP Conf. Ser. 206, High Energy Solar Physics: Anticipating HESSI*, ed. R. Ramaty & N. Mandzhavidze (San Francisco: ASP), 313
 Neidig, D. F., Kiplinger, A. L., Cohl, H. S., & Wiborg, P. H. 1993, *ApJ*, 406, 306
 Ricchiazzi, P. J., & Canfield, R. C. 1983, *ApJ*, 272, 739
 Rosner, R., Tucker, W. H., & Vaiana, G. S. 1978, *ApJ*, 220, 643
 Slottje, C. 1978, *Nature*, 275, 520
 Takakura, T., Nitta, N., Kaufmann, P., Costa, J. E. R., Degaonkar, S. S., & Ohki, K. 1983, *Nature*, 302, 317
 Trottet, G., Rolli, E., Magun, A., Barat, C., Kuznetsov, A., Sunyaev, R., & Terekhov, O. 2000, *A&A*, 356, 1067
 Wang, H., Chae, J., Qiu, J., Lee, C.-Y., & Goode, P. R. 1999, *Sol. Phys.*, 188, 365
 Wang, H., Qiu, J., Denker, C., Spirock, T., Chen, H., & Goode, P. R. 2000, *ApJ*, 542, 1080